**Astronomy
&
Astrophysics**

An X-ray study of the supernova remnant G20.0-0.2 and its surroundings

A. Petriella[1,2], S. A. Paron[1,2,3], and E. B. Giacani[1,3]

[1] Instituto de Astronomía y Física del Espacio (CONICET-UBA), CC 67, Suc. 28, 1428 Buenos Aires, Argentina
e-mail: apetriella@iafe.uba.ar
[2] CBC – Universidad de Buenos Aires, Argentina
[3] FADU – Universidad de Buenos Aires, Argentina

ABSTRACT

Aims. We study the supernova remnant G20.0-0.2 and its surroundings to look for the high-energy counterpart of the radio nebula and to find evidence of interaction between the shock front and the interstellar medium.
Methods. We used *Chandra* archival observations to analyze the X-ray emission from the supernova remnant. The surrounding gas was investigated using data extracted from the Galactic Ring Survey, the VLA Galactic Plane Survey, the Galactic Legacy Infrared Midplane Survey Extraordinaire, and the Bolocam Galactic Plane Survey.
Results. G20.0-0.2 shows diffuse X-ray emission from the central region of the radio remnant. Although the current data do not allow us to distinguish between a thermal or non-thermal origin for the X-ray diffuse emission, based on the radio properties we suggest a synchrotron origin as the most favorable. The hard X-ray point source CXO J182807.4-113516 appears located at the geometrical center of the remnant and is a potential candidate to be the pulsar powering the nebula. We found a molecular cloud adjacent to the flattest border of G20.0-0.2, indicating a probable interaction between the shock front of the remnant and the molecular gas. Several young stellar object candidates are found located in the brightest region of the molecular emission, as well as over a millimeter continuum source and a dark cloud. This distribution is an indication of an active star-forming region around the supernova remnant.

Key words. ISM: supernova remnants – pulsars: general – ISM: clouds – stars: formation

1. Introduction

The supernova remnant (SNR) G20.0-0.2 (hereafter G20) was classified as a plerion[1] by Becker & Helfand (1985) based on the filled-center morphology, the presence of significant polarization at 6 cm, and a flat radio spectral index $\alpha \sim 0.0$ ($S_\nu \propto \nu^\alpha$). In Fig. 1, we show the best image of the radio continuum emission of the SNR at 20 cm, extracted from the MAGPIS (Helfand et al. 2006). The radio synchrotron emission from G20 has a complex morphology, with multiple features like bright knots, arcs, and filaments. The overall emission is dominated by an elliptical central core of about $3\rlap{.}'8 \times 2\rlap{.}'2$, with the major axis oriented in the direction of the Galactic plane. This bright feature is surrounded by faint emission. Two arc-like filaments are located near the outer edges of G20. Interestingly, one border of the SNR is clearly flat and is delineated by a bright radio filament, suggesting that it may have encountered a higher ambient density in this direction.

Pulsar wind nebulae (PWNe) with complex morphologies have been observed in several cases, such as G328.4+0.2 (Gelfand et al. 2007) and G0.9+0.1 (Dubner et al. 2008), but the presence of a flat radio filament is a common characteristic of a surrounding radio shell, with an expected steeper radio spectrum ($\alpha < -0.3$). However, the other available observations at 330 MHz do not have an adequate angular resolution to look for variations in the radio spectral index through the remnant and confirm the presence of a radio shell.

To the north of G20, lies the complex of ultra-compact HII regions GAL 20.08-0.14 (Wood & Churchwell 1989), which appears as a compact and bright radio source adjacent to the SNR. Different masers and molecular lines have been detected toward the HII regions (Avedisova 2002; Galván-Madrid et al. 2009), with velocities between ~40 and ~45 km s^{-1} (all velocities refer to the local standard of rest, hereafter LSR). Anderson et al. (2009) reported the presence of a molecular cloud (MC) that spatially coincides with GAL 20.08-0.14 at a velocity of ~42 km s^{-1}. From an analysis of the HI absorption spectrum, they concluded that the complex of HII regions lies at its far distance, namely, ~12.6 kpc.

In the X-ray domain, the remnant remains almost unexplored. Hands et al. (2002) performed an X-ray survey of selected regions of the Galactic plane with the *XMM-Newton* satellite and reported the presence of some diffuse X-ray emission in the direction of G20. Additionally, the SNR is the only source that lies partially inside the error box of the Fermi-LAT γ-ray source J1828.3-1124c (Nolan et al. 2012). For this reason, the authors suggested a connection between the remnant and the γ-ray emission.

In this work, we present the first X-ray study of the SNR G20.0-0.2 using *Chandra* observations with the aim of establishing whether this remnant is purely plerionic or composite. We also search for source candidates to be the pulsar (PSR) that is powering the emission. In addition, we investigate the interstellar medium around G20, looking for signs of interaction with the expanding shock of the SNR that could explain the peculiar morphology that this remnant shows in the radio band.

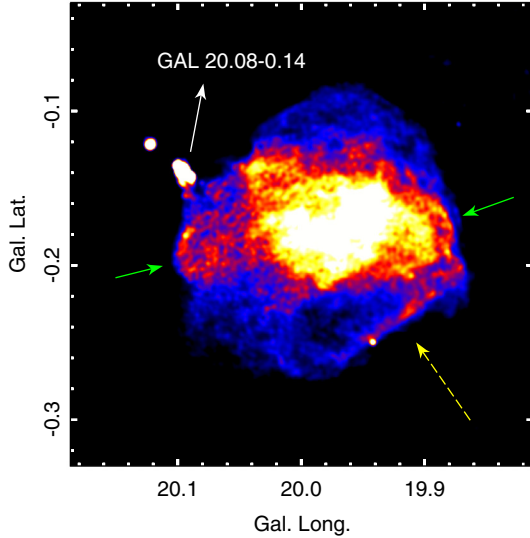[1] Plerions are also referred to as pulsar wind nebulae (PWNe).

Fig. 1. Radio continuum emission of G20.0-0.2 at 20 cm. We marked the position of the complex of UCHII regions GAL 20.08-0.14. The green arrows mark the arc-like filaments and the yellow arrow indicates the flattest border and the radio filament.

2. Results and discussion

2.1. X-ray emission from G20.0-0.2

We reprocessed an archival *Chandra* observation of G20 obtained on 2005 November 5 (ObsID: 5563) using ACIS-I in `vfaint` mode. The data were calibrated with CIAO (version 4.4) and CALDB (version 4.4.8), provided by the Chandra X-ray Center (CXC). After filtering the periods of high count-rate, we produced a cleaned event file with 34.45 ks of observation that was used to perform an imaging and spectral analysis.

2.1.1. Imaging

We analyzed the event file and found an enhancement of the X-ray emission toward the central radio core of G20. We constructed exposure-corrected images in different energy bands and found diffuse emission above 2 keV and a single point source embedded on it. Additionally, we noticed several X-ray clumps outside this extended emission. Most of them are likely point sources that appear broadened by the smoothing. To emphasize the diffuse emission, we produced a point-source subtracted image following the standard procedure described in the Ciao Science Threads. We used the tool `wavdetect` to detect the point source candidates and visually inspected the result to exclude those sources that appear to be actual diffuse emission. For each source, we created the source and background regions with the tool `roi` and replaced the source region with the mean background region using `dmfilth`. To increase the signal-to-noise ratio of the image, we convolved it with a Gaussian kernel. The final image has a spatial scale of 0.05 arcmin/pixel. Figure 2 shows the point sources subtracted X-ray image of the SNR between 2.0 and 7.0 keV, overlaid with some contours of the radio continuum emission. We noticed that the diffuse emission is confined within an ellipse of $1.'8 \times 1.'1$, which is enclosed by the central bright radio core and elongated in the same direction as in the radio band.

Figue 3 shows an X-ray image in the 2.0–7.0 keV energy band toward the diffuse emission. Interestingly, we noted the presence of only one X-ray point source embedded in the diffuse
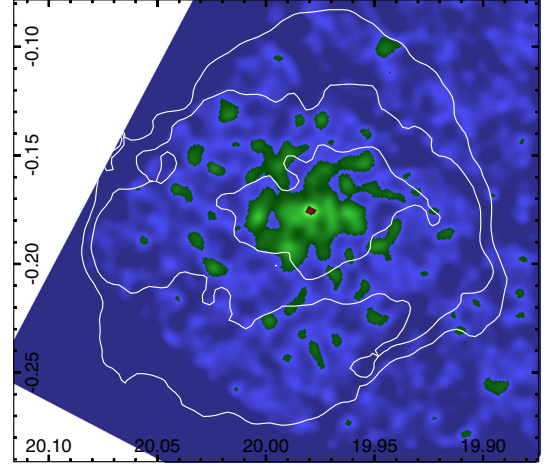
Fig. 2. Exposure-corrected X-ray image between 2.0 and 7.0 keV in Galactic coordinates. Point sources outside the diffuse emission have been subtracted following the procedure described in the text. The contours are the radio continuum emission of the SNR at 20 cm (contour levels are 1.0, 1.7, and 3.0 mJy/beam).
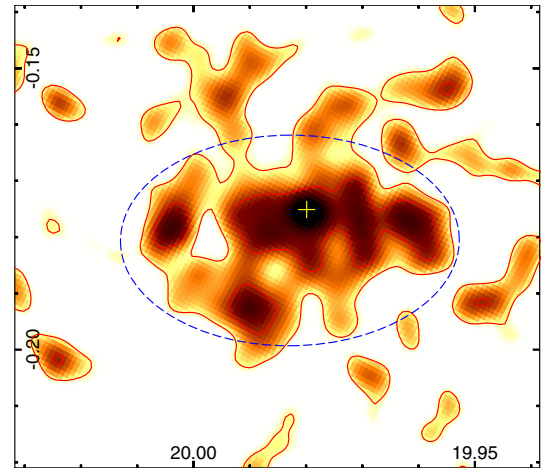

Fig. 3. Exposure-corrected X-ray image between 2.0 and 7.0 keV, enlarged toward the diffuse emission. The yellow cross is CXO J182807.4-113516. The ellipse indicates the region used to extract the spectrum.

X-ray emission (indicated in the figure with a yellow plus sign). This source has been identified in the Chandra Source Catalog (CSC, Evans et al. 2010) as CXO J182807.4-113516 and is centered at RA = $18^h28^m7.43$, Dec = $-11°35'16.''32$, almost at the geometrical center of the radio remnant. In Sect. 2.1.2, we discuss its nature and the connection with the remnant.

2.1.2. X-ray spectral analysis

To perform a spectral analysis of the diffuse emission from the SNR, we extracted the spectrum with the CIAO task `specextract` from the elliptical region indicated in Fig. 3. This region excludes some of the diffuse emission but reduces the contamination from the background. The point source CXO J182807.4-113516 was removed from the extraction region. For the background, we selected a circular region free of diffuse emission and point sources. The spectrum was binned with a minimum of 15 counts/bin. We extracted a total

Table 1. Best-fit parameters for the diffuse X-ray emission of G20.0-0.2 between 1.0 and 7.0 keV.

Model	χ^2/d.o.f.	N_H [$\times 10^{22}$ cm^{-2}]	Γ_X	T_e [keV]	F (1.0–7.0 keV) [$\times 10^{-13}$ erg cm^{-2} s^{-1}]	L (1.0–7.0 keV) [$\times 10^{33}$ erg s^{-1}]
Power law	62.16/62	4*	$1.87^{+0.41}_{-0.44}$	–	$5.29^{+0.93}_{-0.85}$	$1.28^{+0.23}_{-0.20}$
Power law	61.97/61	$3.41^{+2.70}_{-1.65}$	$1.64^{+1.07}_{-0.83}$	–	$4.63^{+4.75}_{-1.37}$	$1.12^{+1.15}_{-0.88}$
Nei	64.84/61	4*	–	$4.97^{+4.06}_{-1.79}$	$5.11^{+0.71}_{-0.71}$	$1.24^{+0.17}_{-0.17}$
Nei	64.83/60	$4.1^{+2.41}_{-1.35}$	–	$4.82^{+7.01}_{-2.40}$	$5.51^{+4.08}_{-1.62}$	$1.34^{+0.98}_{-0.39}$

Notes. The symbol (*) indicates that the parameter was frozen. For the *nei* model, the abundance is solar (from Anders & Grevesse 1989). *F* is the unabsorbed flux. The unabsorbed luminosity *L* was calculated for a distance of 4.5 kpc (see Sect. 2.2). Errors quoted are 90%.
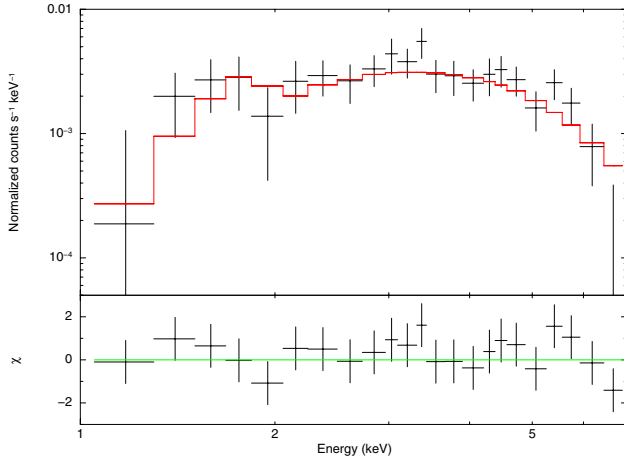

Fig. 4. Chandra ACIS-I spectrum for the diffuse emission from G20.0-0.2. The solid line is the best-fit absorbed power-law model with a hydrogen column density fixed at 4×10^{22} cm^{-2}.

of 1059 counts between 1.0 and 7.0 keV. We fitted the spectrum using XSPEC (version 12.7.1) and χ^2 statistics.

The Chandra ACIS-I spectrum of G20 presents a continuum without evidence of emission lines (Fig. 4). We fitted it with both non-thermal and thermal models. To probe a possible synchrotron origin, we fitted the spectrum with an absorbed power law. For the absorption model (*wabs*), we fixed the hydrogen column density to the value $N_H \sim 4 \times 10^{22}$ cm^{-2}, obtained through the analysis of the neutral and molecular gas (Sect. 2.2). The best fit yields a photon index Γ_X of 1.87, a value similar to that observed in other PWNe (Kargaltsev & Pavlov 2010). Letting the absorption vary freely does not produce any significant improvement in the fitting and results in $N_H \sim 3.4 \times 10^{22}$ cm^{-2}, a value that is still comparable to the one measured using the neutral and molecular data.

Regarding the thermal models, a thermal plasma in collisional equilibrium (*apec*) requires a considerably high electron temperature for an SNR ($T_e \sim 19$ keV) when the abundance parameter is kept equal to the solar value of Anders & Grevesse (1989), as well as a temperature of ~ 7 keV when the abundance is a free parameter. In this last case, although the temperature is not extremely high, the best-fit abundance yields an unrealistic low value ($\sim 10^{-9}$). For a non-equilibrium plasma (*nei*), freezing the abundance to the solar value results in $T_e \sim 5$ keV, which approaches the expected temperature of a young SNR (Vink 2012). The obtained ionization parameter ($\tau < 10^{-9}$ cm^{-3} s) also points to a plasma out of equilibrium. In Table 1, we list the results of the spectral fitting for the power law and the *nei* models.

In conclusion, the spectral fits themselves do not preclude a thermal origin for the X-ray emission from G20. However,

based on the radio properties, we propose that a synchrotron origin for the high-energy emission is the most probable. The mere presence of a PWN component indicates that there is a compact source powering it. The best candidate to be a neutron star is CXO J182807.4-113516, the only X-ray point source embedded in the diffuse emission and located at the geometrical center of the SNR. There is no radio counterpart in the radio image nor any optical or infrared source within the position error box in the USNOb1.0, 2MASS[2], and Spitzer catalogs. The closest point sources are USNOb1.0 0784-0429139, 2MASS 18280728-1135224, and Spitzer G019.9794-00.1736, located at $\sim 9''$, $\sim 6''$, and $\sim 6''$ from CXO J182807.4-113516, respectively. These distances are larger than three times the combined X-ray and optical/infrared positional error.

Although the low number of counts (<20) from CXO J182807.4-113516 does not allow a spectral fitting or timing analysis to be performed to investigate its nature, we can still use the poor spectral information to get a rough picture of this source. We found that all the counts from CXO J182807.4-113516 originate between 3.0 and 8.0 keV, so we defined the hardness ratio H as the ratio of the counts in the 5.0–8.0 keV band to the counts in the 3.0–5.0 keV band. We extracted the net (i.e., background-subtracted) number of counts and obtained 11.82 ± 3.75 counts between 3.0 and 5.0 keV and 6.33 ± 2.73 counts between 5.0 and 8.0 keV, which yields $H = 0.54 \pm 0.29$. This value can be compared with the predicted value of H, which is estimated by assuming different emission models. The X-ray emission from PSRs may correspond either to blackbody emission from the neutron star surface or to non-thermal emission from the magnetosphere. Using the tool W3PIMMS[3] and the net count rate between 3.0 and 8.0 keV (0.00053 cts/s), we modeled the X-ray emission from CXO J182807.4-113516. We fixed the hydrogen column density to 4×10^{22} cm^{-2} to match the absorption of the diffuse emission. For a blackbody with a temperature of 0.1 keV, the predicted H is $\sim 8 \times 10^{-9}$, which is in complete disagreement with the measured value. For a hot blackbody (1 keV), we obtained $H \sim 0.28$, but such high temperature is not expected in a young PSR. According to Kargaltsev & Pavlov (2010), the non-thermal spectrum of a PSR powering a PWN is well described by a power-law model with photon index in the range $1.0 \lesssim \Gamma_X \lesssim 2.0$. The predicted values of H are ~ 0.59 (for $\Gamma_X = 1.0$) and ~ 0.39 (for $\Gamma_X = 2.0$), which are in good agreement with the measured value of $H = 0.54 \pm 0.29$. Thus,

---

[2] The Two Micron All Sky Survey (2MASS) is a joint project of the University of Massachusetts and the Infrared Processing and Analysis Center/California Institute of Technology, funded by the National Aeronautics and Space Administration and the National Science Foundation.
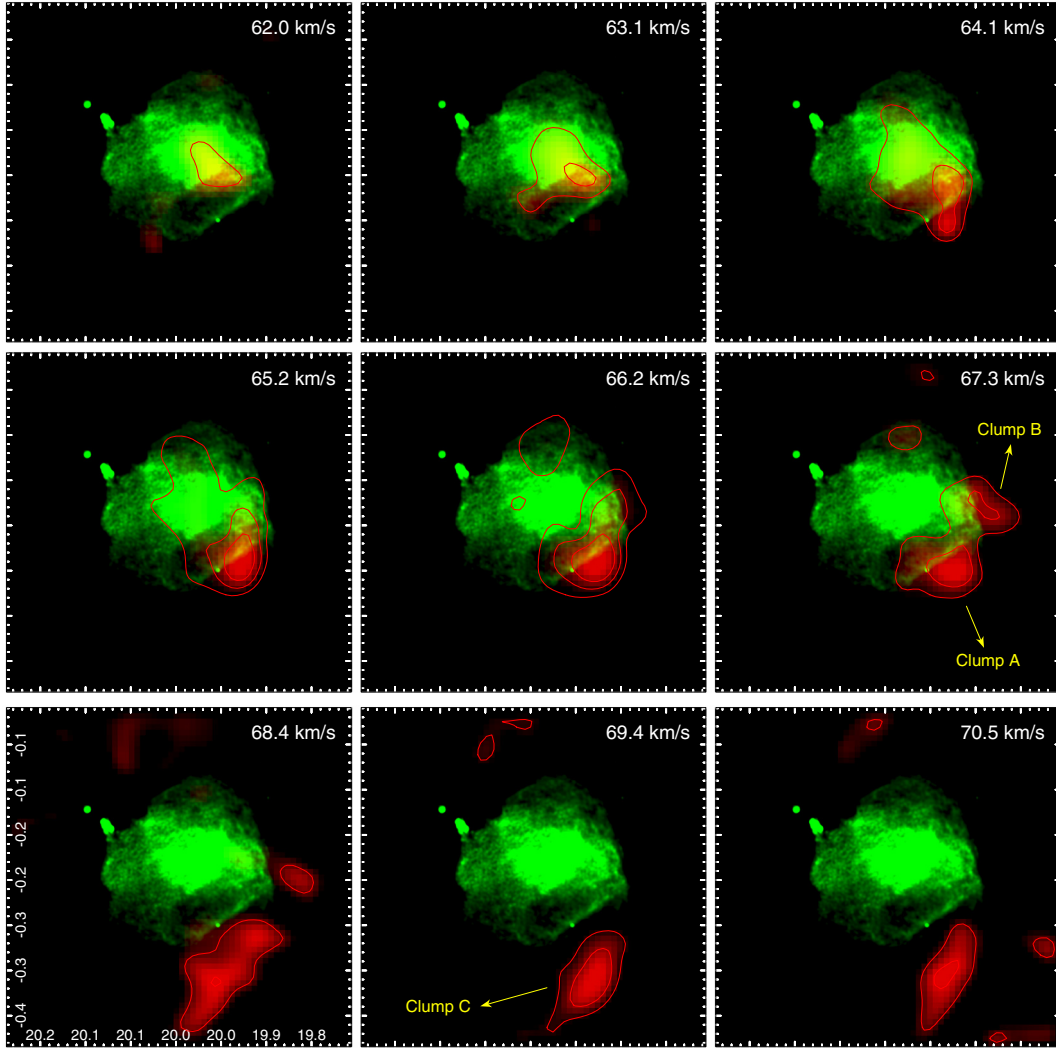
[3] http://heasarc.gsfc.nasa.gov/Tools/w3pimms.html

Fig. 5. Two-color image toward G20.0-0.2 in Galactic coordinates. In red with contours: emission of the ^{13}CO integrated every 1.05 km s^{-1} in the velocity range between 62 km s^{-1} and 71 km s^{-1} (contour levels are 2.7, 4.0, and 5.3 K km s^{-1}). In green: radio continuum emission of G20 at 20 cm. We have marked the two molecular clumps A and B that form the MC probably interacting with the SNR. A third clump (C) appears in the direction of the flattest border of G20 but is not in contact with the remnant.

we conclude that the emission from CXO J182807.4-113516 is more likely non-thermal in origin, although a deeper X-ray exposure of this source is needed to confirm its nature. Using W3PIMM, we estimated its luminosity in the 0.5-8.0 keV band for a distance of 4.5 kpc, obtaining $\sim 0.7 \times 10^{32}$ erg/s (for $\Gamma_X = 1.0$) and $\sim 1.2 \times 10^{32}$ erg/s (for $\Gamma_X = 2.0$). From the best-fit power-law model, the X-ray luminosity of G20 between 0.5 and 8.0 keV is $\sim 1.8 \times 10^{33}$ erg/s. The luminosities of G20 and CXO J182807.4-113516 are in good agreement with those reported by Kargaltsev & Pavlov (2010) for other PWNe and their powering PSRs. Thus, based on its position and spectral behavior, CXO J182807.4-113516 appears as a good candidate to be the PSR created after the explosion of the supernova that originated G20 and that is powering the synchrotron nebula.

2.2. The interstellar medium around G20.0-0.2

We studied the interstellar medium around G20 to investigate the presence of MCs that may have affected the expansion of the SNR shock front. The molecular data were extracted from the Galactic Ring Survey (GRS, Jackson et al. 2006). The survey

maps the Galactic ring in the ^{13}CO $J = 1–0$ line with angular and spectral resolutions of 46″ and 0.2 km s^{-1}, respectively. The observations were performed in both position-switching and on-the-fly mapping modes, achieving an angular sampling of 22″.

By inspecting the whole ^{13}CO cube, we found a molecular feature extending from 62 to 71 km s^{-1} as the most probable structure to be in contact with the SNR. In Fig. 5, we present the ^{13}CO emission integrated every 1.05 km $^{-1}$ along this velocity range, displayed in Galactic coordinates. We noted the presence of a cloud that shows an arc-shape morphology and delineates the southern border of the SNR. This cloud is composed of two molecular clumps, labeled A and B. Molecular clump A lies right upon the flattest border of G20 (we refer to Fig. 1), while clump B is located adjacent to the southeastern border of the SNR. A third molecular structure (labeled clump C) appears in the direction of the flattest border, but is not in contact with the radio emission.

The molecular clump A spatially coincides with the Bolocam Galactic Plane Survey (BGPS)[4] millimeter continuum source

---

[4] The BGPS is a 1.1 mm continuum survey of the Galactic plane made using Bolocam on the Caltech Submillimeter Observatory, with a 33″ FWHM effective resolution (Aguirre et al. 2011).
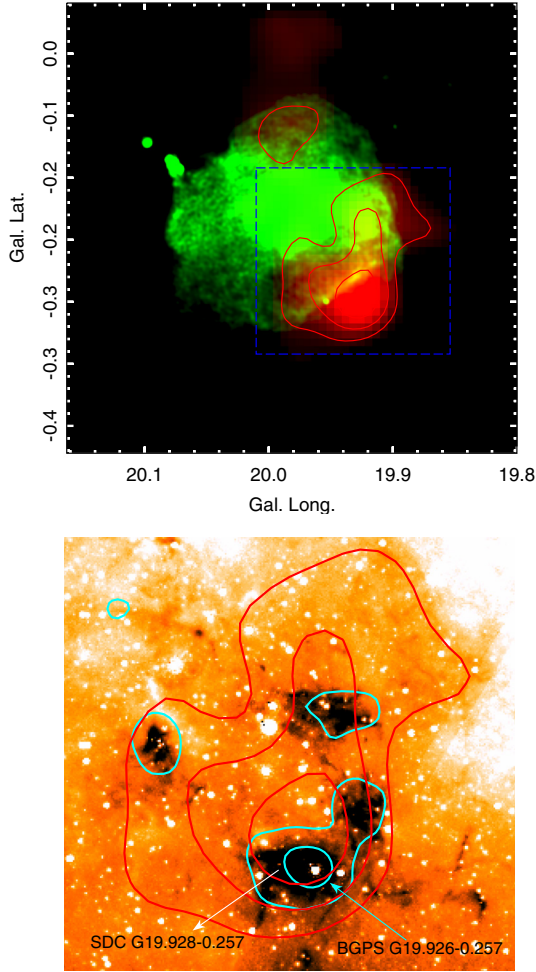
Fig. 6. *Top*: two-color image toward G20.0-0.2. In green: radio continuum emission at 20 cm. In red: emission of the ^{13}CO integrated between 64.3 and 68.6 km s^{-1} (contour levels are 10.0, 14.6, and 19.0 K km s^{-1}). The blue rectangle indicates the area shown in the adjacent figure. *Bottom*: *Spitzer*-IRAC 8 μm band. The red contours are the ^{13}CO emission and the cyan contours are the 1.1 mm continuum emission from the BGPS (contour levels are 0.1 and 0.5 Jy/Beam). The most intense molecular emission (traced by the 19.0 K km s^{-1} contour level) shows a spatial correspondence with the millimeter source BGPS G19.926-0.257 and the dark cloud SDC G19.928-0.257.

BGPS G19.926-0.257. Besides, this source lies within the ellipse of the Spitzer dark cloud SDC G19.928-0.257 (Peretto & Fuller 2009). In Fig. 6, we show the excellent spatial correspondence among the molecular emission, the millimeter continuum source, and the dark cloud.

Analyzing the ^{13}CO spectra toward the borders of the SNR, we found some interesting spectral features. Figure 7 displays an averaged spectrum obtained from a region toward the SNR's flattest border, centered at $l = 19.944°$, $b = −0.245°$. The spectrum is not symmetric and presents a slight spectral shoulder toward higher velocities. The red curve in the figure is the result of the fitting with two Gaussian functions with central velocities and FWHM Δv of 65.3 and 68.5 km s^{-1}, and 3.8 and 5.0 km s^{-1}, respectively. Such asymmetry could be evidence of turbulent motion in the gas, maybe produced by the SNR shock (see, e.g., Falgarone et al. 1994), although we can not discard the presence of multiple molecular components.

Assuming that 66 km s^{-1} is the central velocity of the cloud, according to the Galactic model of Fich et al. (1989), this cloud
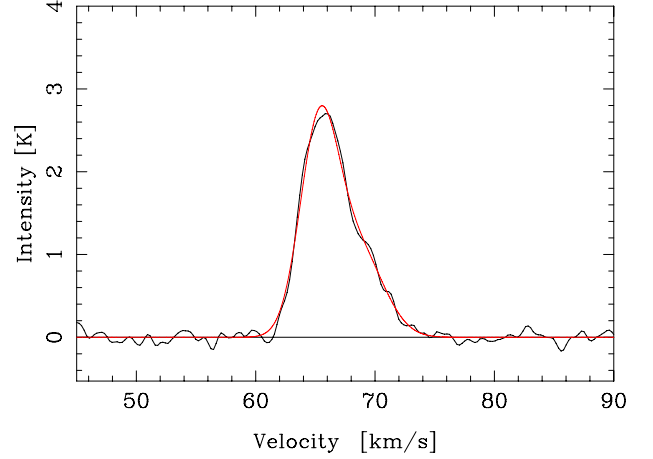

Fig. 7. Averaged spectrum obtained from a region toward the SNR flattest border, centered at $l = 19.944°$, $b = −0.245°$. The fit with two Gaussian functions is shown in red.
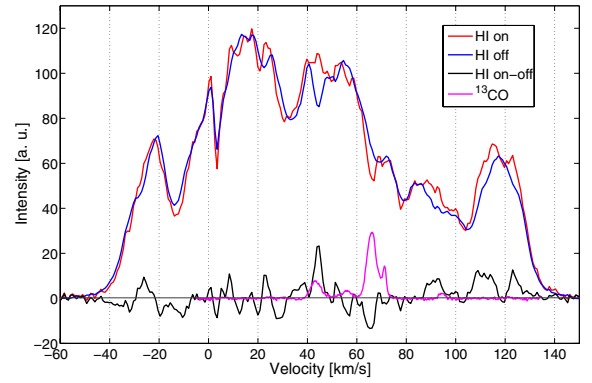

Fig. 8. ^{13}CO and HI spectra toward molecular clump A: ^{13}CO emission spectrum (magenta), HI on-position spectrum (red), HI off-position spectrum (blue), and HI absorption spectrum on-off (black).

could be located at the distances of either 4.5 and 11.5 kpc. To resolve the ambiguity, we followed the procedure described in Roman-Duval et al. (2009). An MC have HI embedded within it, which is cooler than the Galactic inter-cloud HI. Therefore, an MC located at the near distance absorbs the radiation from the warm HI at the far distance with the same velocity. As a consequence, the HI spectrum toward an MC at the near distance shows an absorption feature whose velocity coincides with the velocity of the molecular emission line.

We constructed an HI absorption spectrum toward the clump A, which presents the most convincing signature of interaction with the SNR. The HI data were extracted from the Very Large Array Galactic Plane Survey (VGPS, Stil et al. 2006), which maps the HI 21 cm line emission with angular and spectral resolutions of 1′ and 1.3 km s^{-1}, respectively. We obtained the ^{13}CO and HI on-position spectra from a rectangular region within the 19 K km s^{-1} contour level (see Fig. 6, top) and outside the SNR to avoid the effect of the radio continuum source in the absorption spectrum. The off-position HI spectrum was made by averaging three HI spectrum from rectangular regions adjacent to clump A and free of ^{13}CO emission. The HI absorption spectrum results from the subtraction of the HI on- and off-position spectra. In Fig. 8, we show the HI and ^{13}CO spectra toward the molecular clump A. We noted the presence of an HI absorption line at a velocity of ~65 km s^{-1}, which coincides with a ^{13}CO emission line from the cloud. From this analysis, we favor

Table 2. Physical characteristics of molecular clumps A and B.

Clump	v_c [km s^{-1}]	Δv [km s^{-1}]	Size [arcmin (pc)]	$N(H_2)$ [$\times 10^{21}$ cm^{-2}]	Mass [$M_\odot$]	Density [cm^{-3}]
A	~66	6	2.8×3.8 (3.7×5.0)	9.9	12 700	550
B	~69	4	4.3×2.2 (5.6×2.9)	4.0	4500	230

Notes. LSR central velocity (v_c), velocity width (Δv), size, H$_2$ column density, mass, and number density. The linear size, mass, and number density were calculated assuming a distance of 4.5 kpc.

the near distance of 4.5 kpc for molecular clump A and thus for the SNR G20.0-0.2.

An additional evidence that the near kinematic distance could be the most likely one is the presence of the millimeter source BGPS 019.926-00.257 lying inside the Spitzer dark cloud SDC G19.928-0.257, both of them associated with the molecular clump A (see Fig. 6, bottom). In fact, dark clouds are clouds of dust that appear dark as they absorb the mid-infrared radiation of the Galaxy. For this reason, they are usually placed at the near kinematic distance (Schlingman et al. 2011). Thus, we consider that the SNR (located at ~4.5 kpc) and the UC HII region complex GAL 20.08-0.14 (at ~12.6 kpc) are not related.

To estimate the mass and density of the molecular clumps, we assumed local thermodynamic equilibrium (LTE). For the ^{13}CO column density we used

$$N\left(^{13}\mathrm{CO}\right) = 2.42 \times 10^{14} \frac{T_{ex} + 0.88}{1 - e^{-5.29/T_{ex}}} \int \tau_{13} \mathrm{d}v, \tag{1}$$

where T_{ex} is the excitation temperature of the ^{13}CO transition and τ_{13} is the optical depth of the line. Assuming that the ^{13}CO $J = 1$–0 line is optically thin, we used the approximation

$$\int \tau_{13} \mathrm{d}v \sim \frac{1}{J(T_{ex}) - J(T_b)} \int T_B \mathrm{d}v, \tag{2}$$

where $J(T) = 5.29(e^{5.29/T} - 1)^{-1}$, $T_b = 2.7$ K is the background temperature, and T_B is the brightness temperature of the line. To obtain the H$_2$ column density, we took the relative abundance from Simon et al. (2001): $N(H_2)/N(^{13}\mathrm{CO}) \sim 5 \times 10^5$. The mass of the molecular clumps was calculated from

$$M = \mu\, m_H \sum \left[D^2\, \Omega\, N(H_2) \right], \tag{3}$$

where Ω is the solid angle subtended by the ^{13}CO $J = 1$–0 beam size, m_H is the hydrogen mass, μ is the mean molecular weight assumed to be 2.8 by taking into account a relative helium abundance of 25%. Our summation was performed over the area of each molecular clump. The column density was calculated assuming $T_{ex} = 10$ K and the mass and number density considering a distance of 4.5 kpc. In Table 2, we report the physical parameters of the molecular clumps A and B. The obtained masses and densities are similar to those measured toward other MCs interacting with SNRs (see Paron et al. 2012; Dubner et al. 2004).

Additionally, we calculated the total hydrogen column density $N(H)$, which is an important parameter in the modeling of X-ray emission (see Sect. 2.1.2). For this purpose, we summed the contributions from both neutral and molecular hydrogen column densities: $N(H) = N(HI) + 2N(H_2)$. The integration was performed in the velocity range between 0 and 66 km s^{-1} and over the central core, in a region delimited by the 3.0 mJy/beam contour level of the radio continuum emission (see Fig. 2),

where the diffuse X-rays originate. The molecular column density $N(H_2)$ was obtained from Eq. (1) and the neutral column density $N(HI)$ from the following equation:

$$N(HI) = 1.82 \times 10^{21} \int T_B \mathrm{d}v. \tag{4}$$

We obtained $N(H) \sim 4 \times 10^{22}$ cm^{-2}.

2.3. Young stellar objects embedded in the molecular gas

The expansion of the shock front of an SNR into the interstellar medium gives rise to a broad range of phenomena. An SNR can compress MCs and induce the formation of inhomogeneities in the gas, which may collapse into dense molecular clumps where, eventually, new stars may form. Up to the present, there is no conclusive observational evidence indicating that the SNRs can trigger star formation. Only a few studies have revealed the existence of young stellar objects (YSOs) in the periphery of SNRs, such as the filled-center remnants G24.7+0.6 (Petriella et al. 2010) and G54.1+0.3 (Koo et al. 2008) and the shell-type G59.5+0.1 (Xu & Wang 2012), G0.1-0.1, G6.41-0.1 (W28), and G355.9-2.5 (Marquez-Lugo & Phillips 2010). The main controversy regarding star formation triggered by an SNR is the difference between two timescales, namely, the SNR's age (~10^5 yr) and the YSO's characteristic age (~10^6 yr), which would make it impossible to directly observe an SNR inducing the collapse of molecular cores to form new stars. However, the progenitors of core-collapse supernovae are massive stars, whose strong stellar wind during the duration of the main sequence phase ($\gtrsim 10^6$ yr) can provide additional injection of energy into the molecular gas prior to the SNR.

In the case of G20, the radio and X-ray properties indicate that it is a core-collapse SNR. In addition, we showed that the remnant is very likely interacting with an MC. So, it appears to be a proper candidate to study star-forming activity in its vicinity. To look for YSO candidates around G20, we constructed a color-color (cc) diagram in the *Spitzer*-IRAC bands [5.8]–[8.0] vs. [3.6]–[4.5] (not shown here) with sources that report flux measurements in the four bands. We applied the criterion of Allen et al. (2004) to identify class I YSO candidates, i.e., young stars at the earlier stages of evolution. In Fig. 9, we show the distribution of the class I YSO candidates, overimposed to the MC probably interacting with G20. From this figure, we noted the presence of several clusters of YSO candidates, but we call special attention to a group of six YSO candidates that appear projected on the clump A, which is associated with the millimeter source BGPS G19.926-0.257 and with the dark cloud SDC G19.928-0.257. The presence of dense molecular material, a dark cloud, abundant dust (traced by the millimeter source), and YSO candidates suggests that this region could be an active star-forming site (Rathborne et al. 2007, 2006), representing another potential site of star formation near an SNR.
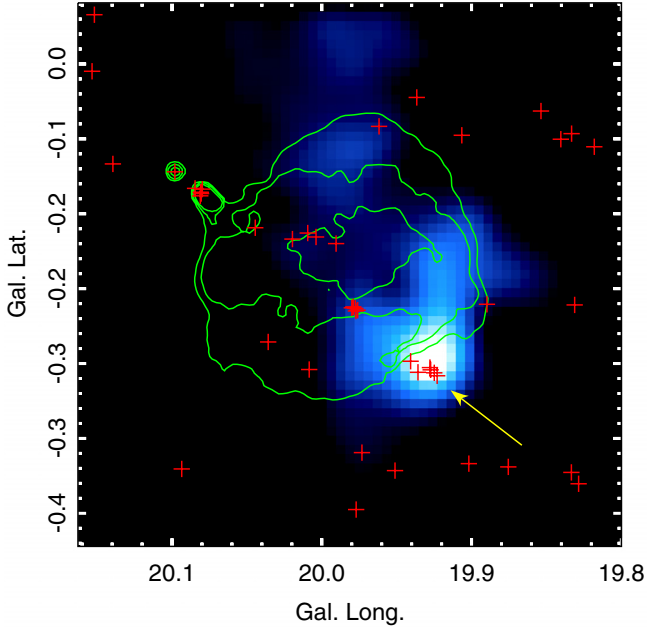
3. Concluding remarks

We have presented the first X-ray study of the SNR G20.0-0.2 using *Chandra* observations. We detected diffuse emission, which has a very good correlation with the bright central radio emission. The X-ray spectrum can be equally well fitted by a thermal plasma in a non-equilibrium or a power-law model. Taking into account the obtained photon index $\Gamma_X \sim 1.9$ and the radio properties of the SNR, we conclude that a non-thermal origin of the X-ray emission is the most probable. In addition, we have reported the presence of the hard X-ray point source CXO J182807.4-113516 located at the geometrical center of the remnant, which is characterized by a non-thermal spectrum and an X-ray luminosity between $\sim 0.7–1.2 \times 10^{32}$ erg/s in the 0.5–8.0 keV band (similar to young PSRs), suggesting that it is a good candidate to be the central compact source powering the PWN.

The study of the surrounding interstellar gas around G20 allowed us to constrain its distance to a value of 4.5 kpc. We found an MC with some indications of interaction with the flattest border of the radio emission, and in excellent spatial correspondence with the millimeter continuum source BGPS G19.926-0.257 and the dark cloud SDC G19.928-0.257. We identified a group of class I YSO candidates located in the brightest region of the MC. The presence of these young sources, a dark cloud, and abundant dust suggest that the region around G20 could be a potential star-forming site.

References

Aguirre, J. E., Ginsburg, A. G., Dunham, M. K., et al. 2011, ApJS, 192, 4
Allen, L. E., Calvet, N., D'Alessio, P., et al. 2004, ApJS, 154, 363
Anders, E., & Grevesse, N. 1989, Geochim. Cosmochim. Acta, 53, 197
Anderson, L. D., Bania, T. M., Jackson, J. M., et al. 2009, ApJS, 181, 255
Avedisova, V. S. 2002, VizieR Online Data Catalog: V/112A
Becker, R. H., & Helfand, D. J. 1985, ApJ, 297, L25
Dubner, G., Giacani, E., Reynoso, E., & Parón, S. 2004, A&A, 426, 201
Dubner, G., Giacani, E., & Decourchelle, A. 2008, A&A, 487, 1033
Evans, I. N., Primini, F. A., Glotfelty, K. J., et al. 2010, ApJS, 189, 37
Falgarone, E., Lis, D. C., Phillips, T. G., et al. 1994, ApJ, 436, 728
Fich, M., Blitz, L., & Stark, A. A. 1989, ApJ, 342, 272
Galván-Madrid, R., Keto, E., Zhang, Q., et al. 2009, ApJ, 706, 1036
Gelfand, J. D., Gaensler, B. M., Slane, P. O., et al. 2007, ApJ, 663, 468
Hands, A., Warwick, R., Watson, M., & Helfand, D. 2002
    [arXiv:astro-ph/0202180]
Helfand, D. J., Becker, R. H., White, R. L., Fallon, A., & Tuttle, S. 2006, AJ,
    131, 2525
Jackson, J. M., Rathborne, J. M., Shah, R. Y., et al. 2006, ApJS, 163, 145
Kargaltsev, O., & Pavlov, G. G. 2010, X-ray Astronomy 2009; Present Status,
    Multi-Wavelength Approach and Future Perspectives, 1248, 25
Koo, B.-C., McKee, C. F., Lee, J.-J., et al. 2008, ApJ, 673, L147
Marquez-Lugo, R. A., & Phillips, J. P. 2010, MNRAS, 407, 94
Nolan, P. L., Abdo, A. A., Ackermann, M., et al. 2012, ApJS, 199, 31
Paron, S., Ortega, M. E., Petriella, A., et al. 2012, A&A, 547, A60
Peretto, N., & Fuller, G. A. 2009, VizieR Online Data Catalog: J/A+A/505/405
Petriella, A., Paron, S., & Giacani, E. 2010, Boletin de la Asociacion Argentina
    de Astronomia, 53, 221
Rathborne, J. M., Jackson, J. M., & Simon, R. 2006, ApJ, 641, 389
Rathborne, J. M., Simon, R., & Jackson, J. M. 2007, ApJ, 662, 1082
Roman-Duval, J., Jackson, J. M., Heyer, M., et al. 2009, ApJ, 699, 1153
Schlingman, W. M., Shirley, Y. L., Schenk, D. E., et al. 2011, ApJS, 195, 14
Simon, R., Jackson, J. M., Clemens, D. P., Bania, T. M., & Heyer, M. H. 2001,
    ApJ, 551, 747
Stil, J. M., Taylor, A. R., Dickey, J. M., et al. 2006, AJ, 132, 1158
Vink, J. 2012, A&ARv, 20, 49
Wood, D. O. S., & Churchwell, E. 1989, ApJS, 69, 831
Xu, J.-L., & Wang, J.-J. 2012, A&A, 543, A24